

## Aberrant neural and cardiac development in mice lacking the ErbB4 neuregulin receptor

Martin Gassmann\*, Franca Casagrande†, Donata Orioli†, Horst Simon\*, Cary Lai‡, Rüdiger Klein† & Greg Lemke\*§

\* Molecular Neurobiology Laboratory, Salk Institute for Biological Studies, La Jolla, California 92037, USA

† Differentiation Program, European Molecular Biology Laboratory, 69012 Heidelberg, Germany

‡ Department of Neuropharmacology, Scripps Research Institute, La Jolla, California 92037, USA

VARIOUS *in vitro* studies have suggested that ErbB4 (HER4) is a receptor for the neuregulins, a family of closely related proteins implicated as regulators of neural and muscle development, and of the differentiation and oncogenic transformation of mammary epithelia<sup>1-3</sup>. Here we demonstrate that ErbB4 is an essential *in vivo* regulator of both cardiac muscle differentiation and axon guidance in the central nervous system (CNS). Mice lacking ErbB4 die during mid-embryogenesis from the aborted development of myocardial trabeculae in the heart ventricle. They also display striking alterations in innervation of the hindbrain in the CNS that are consistent with the restricted expression of the *ErbB4* gene in rhombomeres 3 and 5. Similarities in the cardiac phenotype of *ErbB4* and *neuregulin* gene mutants suggest that ErbB4 functions as a neuregulin receptor in the heart; however, differences in the hindbrain phenotypes of these mutants are consistent with the action of a new ErbB4 ligand in the CNS.

ErbB4 (HER4), ErbB3 (HER3) and ErbB2 (HER2, Neu) are a family of cell-surface receptors that exhibit structural similarity to the receptor for epidermal growth factor (EGF)<sup>4-6</sup>. Although these proteins have been intensively studied in a variety of biological contexts in cell culture, their action and interaction during mammalian development *in vivo* are largely unknown. In cultured cells, the ligands for the ErbB2/3/4 receptors are the neuregulins<sup>1,7</sup>, a set of proteins also referred to as glial growth factors (GGFs)<sup>8,9</sup>, Neu differentiation factors (NDFs)<sup>10</sup>, heregulins (HRGs)<sup>11</sup> and acetylcholine receptor inducing activity (ARIA)<sup>12</sup>. This surfeit of names reflects the diverse biological activities of the neuregulins *in vitro*, as glial cell mitogens, receptor binding proteins, mammary differentiation factors, and muscle trophic factors.

We sought to assess the *in vivo* action of the most functionally independent of the neuregulin receptors—ErbB4 (ref. 1)—through the generation of loss-of-function mutations in the mouse *ErbB4* gene. We isolated genomic clones of this gene from a strain 129/Sv genomic library, prepared the pPNT-based targeting vector (Fig. 1a)<sup>13</sup>, electroporated this construct into the R1 line of mouse embryonic stem (ES) cells<sup>14</sup>, and identified clonal lines in which the mutated *ErbB4* allele had replaced one of the wild-type *ErbB4* alleles through homologous recombination (Fig. 1b). Selected ES cell clones were microinjected into C57BL/6J blastocysts, which were then transferred to pseudo-pregnant females to generate chimaeric mice. Breeding of these chimaeras to C57BL/6J mice resulted in germline transmission of the *ErbB4* mutation. Mice heterozygous for the inactivated *ErbB4* allele displayed no obvious behavioural or anatomical defects. When these heterozygotes were crossed, however, we observed no homozygous mutants in any of the newborn litters examined. Closer inspection showed that all *ErbB4*<sup>-/-</sup> homozygotes died *in utero*, between 10 and 11 days after fertilization (E10–11). As expected from the design of the targeting vector (see Fig. 1), these homozygotes expressed no detectable ErbB4

§ To whom correspondence should be addressed.

protein, as assessed by western blot with an ErbB4 antibody (Fig. 1c) or *ErbB4* messenger RNA, as assessed by whole-mount *in situ* hybridization (see below).

The mid-embryonic lethality of *ErbB4*<sup>-/-</sup> mice results from the aborted development of heart muscle. This phenotype is consistent with the normal pattern of *ErbB4* gene expression at E9.5, which is largely confined to cardiac muscle and the nervous system (Fig. 2). Within the heart, *ErbB4* mRNA is present throughout both the atrial and ventricular myocardium (muscle), but is absent from the endocardium, which is the endo-

thelial lining of the organ (Fig. 2c). (These endothelial cells are the site of *neuregulin* gene expression<sup>15</sup>.) *ErbB4* mRNA is present in both the myocardium of the developing chamber walls and in the myocardial cells that make up the trabeculae<sup>16</sup>, which are the interlinked finger-like projections of heart muscle that extend from the ventricular wall into the interior of the chamber (Figs 2d and 3a). We found that the E10.5 hearts of *ErbB4*<sup>-/-</sup> mice contain intact, apparently normal, chamber walls but are devoid of ventricular trabeculae (Fig. 3a, b). The endocardium appears to be normally configured in the mutants, although the endo-

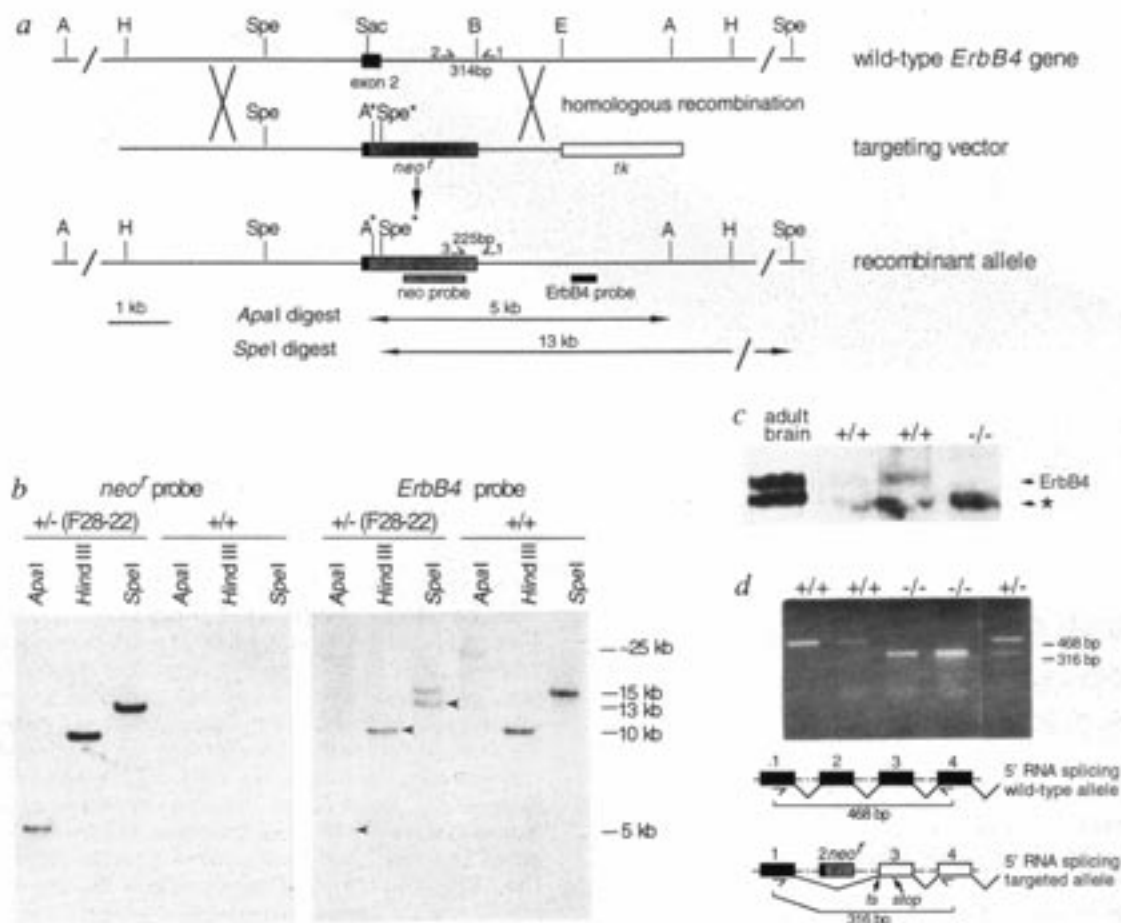
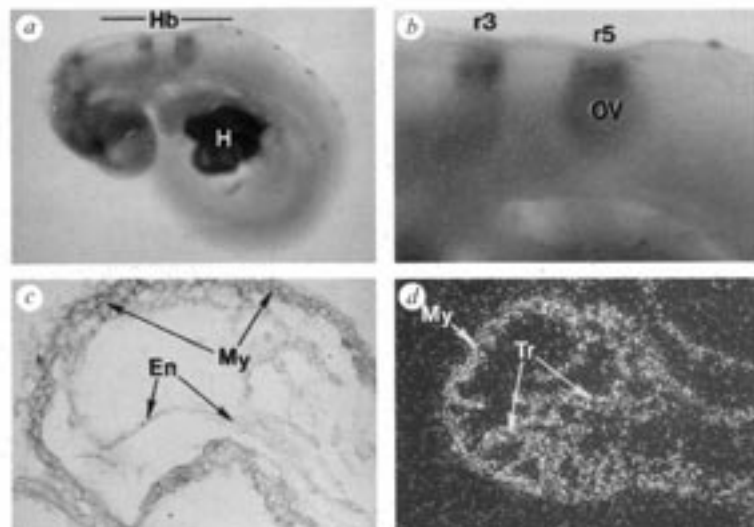


**FIG. 1** Mouse *ErbB4* gene targeting. **a**, Structure of the mouse *ErbB4* gene around exon 2, of the targeting construct for homologous recombination, and of the recombinant allele. The *ErbB4* gene is >100 kb in length, and the  $\lambda$  phage clone used for preparation of the targeting construct contains only coding sequence from the second exon of the gene (M. Gassmann, unpublished data). Abbreviations: A, *Apal*; H, *HindIII*; Spe, *SpeI*; Sac, *SacI*; B, *BamHI*; E, *EcoRI*; *neo*<sup>r</sup>, G418 resistance cassette for positive selection of homologous ES cell recombinants; *tk*, herpes simplex virus thymidine kinase gene for selection against non-homologous recombinants. The *neo* and *ErbB4* probes used for the Southern blots of **b**, and the polymerase chain reaction (PCR) primers (arrows 1, 2 and 3) used for routine genotyping of embryos, are indicated. New *Apal* and *SpeI* sites introduced through homologous recombination are indicated by asterisks. **b**, Southern blots of genomic DNA from wild-type ES cells (+/+) and from F28-22 ES cells heterozygous for the recombinant *ErbB4* allele (+/-), hybridized with either the *neo*<sup>r</sup> (left) or *ErbB4* (right) probes indicated in **a**. Arrowheads in the *ErbB4* blot indicate hybridizing bands corresponding to the recombinant allele. The arrowed *HindIII* band of +/- DNA in the *ErbB4* blot is a doublet. **c**, Western blot of proteins extracted from adult mouse brain, and from wild-type (+/+) and *ErbB4* mutant (-/-) E10.5 mouse embryos, probed with an anti-ErbB4 rabbit antiserum (C. Lai, unpublished results). The p180 ErbB4 band and a crossreacting non-ErbB4 band (asterisk) are indicated. **d**, Top, reverse transcription (RT)-PCR of RNA extracted

from whole E10.5 wild-type (+/+), heterozygous (+/-) and *ErbB4* mutant (-/-) mouse embryos. *ErbB4*<sup>-/-</sup> embryos contain a low level of mis-spliced, frameshifted *ErbB4* RNA that is not detectable by *in situ* hybridization. Bottom, diagram of deduced 5' splicing reactions, based on cloning and DNA sequencing of the 468-bp and 316-bp PCR products illustrated above, and comparison of these sequences to the previously mapped splice junctions flanking *ErbB4* exons 1-4 (M. Gassmann, unpublished results). Arrows indicate the position of the exon 1 and exon 4 primers used for RT-PCR; fs, frameshift.

**METHODS.** Southern blot hybridizations were performed according to standard protocols. Blots were hybridized with the indicated <sup>32</sup>P-dCTP-labelled probes. Western blots were performed according to standard protocols, and were reacted with an affinity-purified rabbit antiserum generated against a glutathione-S-transferase fusion protein containing carboxy-terminal-proximal amino acids of the mouse ErbB4 protein corresponding to residues 1185-1238 of the human ErbB4 sequence (C. Lai, unpublished data). Blots were developed with an ECL chemiluminescent detection system. RT-PCR was performed according to standard protocols, starting with ~5  $\mu$ g of total RNA isolated from whole mouse embryos. PCR was performed for 30 cycles, using upstream and downstream primers (arrows) corresponding to positions (-12)-12 and 456-433, respectively, from the start codon of the mouse *ErbB4* cDNA (C. Lai, unpublished results). Amplified DNAs were subcloned into pCR-Script (Stratagene) and sequenced.

**FIG. 2** Expression of the wild-type *ErbB4* gene in E9.5 mouse embryos. **a**, Low-power view (anterior to the left) of an entire E9.5 embryo in which *ErbB4* mRNA (dark purple reaction product) is visualized with digoxigenin-based whole-mount *in situ* hybridization. *ErbB4* mRNA is evident in the heart (H) and rostral CNS, with two stripes of expression in segments of the hindbrain (Hb). **b**, Higher magnification view of the E9.5 hindbrain. *ErbB4* mRNA is confined to the dorsal regions of rhombomeres 3 and 5 (r3 and r5), the latter of which is positioned adjacent to the otic vesicle (OV). **c**, Sagittal section of an E9.5 heart (ventricle) from the embryo previously analysed by whole-mount *in situ* hybridization as in **a**. Ventricular trabeculation (see text) begins around this time. *ErbB4* mRNA is detectable in the myocardium (My), but not in the endocardium (En) that lines the ventricle. **d**, Sagittal section of a slightly older (E10.5) heart ventricle in which the formation of trabeculae (Tr) is well advanced. *ErbB4* mRNA, detected as white grains with  $^{35}\text{S}$  *in situ* hybridization, is now apparent in both the myocardial wall (My) and the developing myocardial trabeculae.



**METHODS.** Whole-mount *in situ* hybridization with digoxigenin-labelled probes and detection with AP-conjugated antibody (Boehringer-Mannheim) was performed as described previously<sup>28</sup>. After visualization, embryos were embedded in paraffin and sections were cut at 8  $\mu\text{m}$ . For  $^{35}\text{S}$  *in situ* hybridization embryos were fixed at 4% paraformaldehyde, immersed in 20% sucrose/PBS for 24 h and were subsequently embedded in OCT (Tissue-Tek). Hybridization to 14- $\mu\text{m}$  cryosections was performed as described

previously<sup>29,30</sup>, using  $^{35}\text{S}$ -radiolabelled antisense and sense (control) RNAs transcribed *in situ* from a 5' mouse *ErbB4* cDNA fragment subcloned into pCR-Script.

cardial cushion, from which the heart valves eventually develop, is often slightly reduced in size relative to wild type (Fig. 3b). The failure of trabeculation in *ErbB4*<sup>-/-</sup> mice leads to severely reduced embryonic blood flow: note the greater number of red blood cells present in the mutant heart (Fig. 3b) relative to wild type (Fig. 3a). The E10.5 embryonic lethality and lack of cardiac trabeculation that we observe in *ErbB4*<sup>-/-</sup> mice are also prominent features of mice homozygous for loss-of-function mutations in either the *neuregulin* or *ErbB2* genes (see refs 17, 18).

In the E9.5 nervous system, *ErbB4* expression is observed in the hindbrain (Fig. 2b), the midbrain and the ventral forebrain

(Fig. 2a). Expression in the E9.5 hindbrain is precisely localized to two segments—rhombomeres 3 and 5—and is further restricted within these rhombomeres to the dorsal third of the neural tube (Fig. 2b) and to two symmetric pools of cells immediately above the developing ventral motor neurons (data not shown). The flanking segments that lack *ErbB4* mRNA—rhombomeres 2, 4 and 6—are associated with streams of neural crest cells that populate cranial sensory ganglia V (trigeminal), VII and VIII (facial and acoustic), and IX (glossopharyngeal) of the peripheral nervous system (PNS), respectively<sup>19,20</sup>. We examined the organization and innervation of these ganglia in wild-type

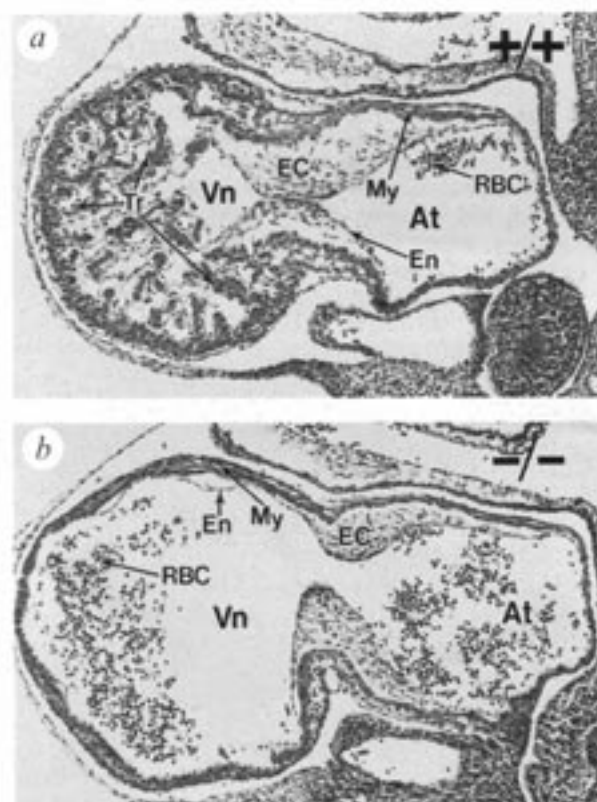
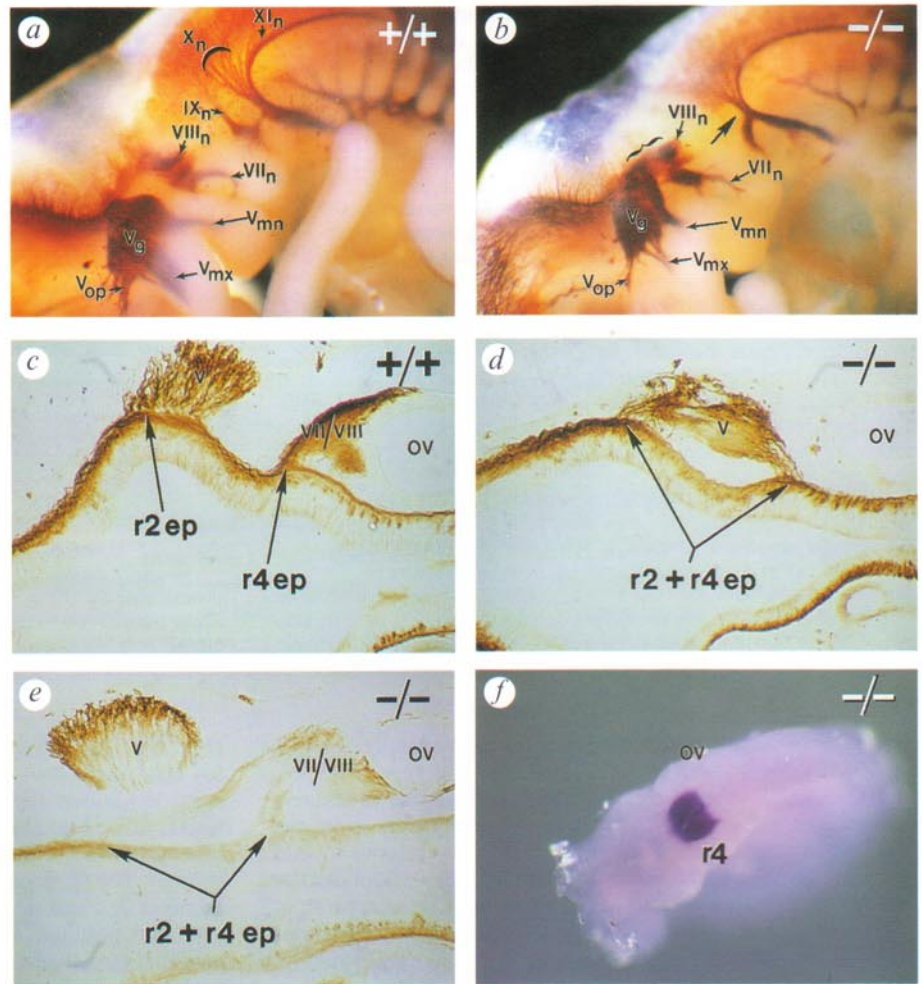
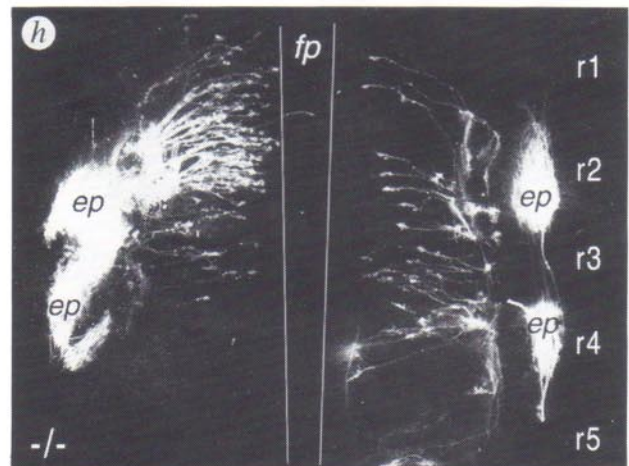
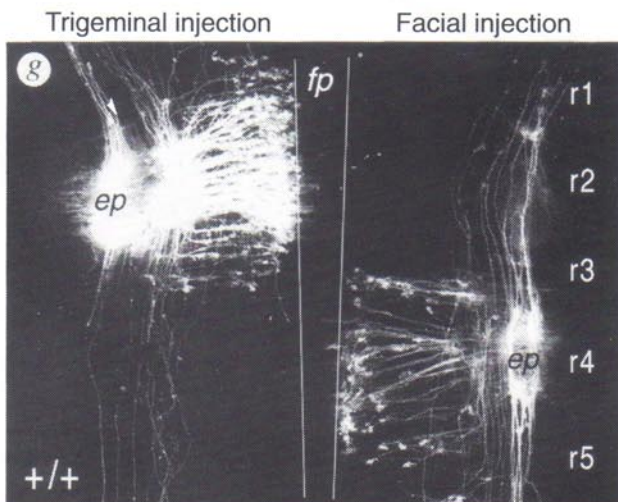


**FIG. 3** Histology of wild-type and mutant mouse hearts at embryonic day 10.5. **a**, A sagittal section through the centre of wild-type (+/+) heart, in which the ventricle (Vn) and atrium (At) are separated by the endocardial cushion (EC). The outer myocardial (My) muscle and inner endocardial (En) endothelial tissues are readily distinguished, and elaborate myocardial trabeculae (Tr), draped by a layer of endocardial cells, are apparent in the ventricle. The atrium contains a small pool of red blood cells (RBCs). **b**, An equivalent sagittal section through the same region of an *ErbB4* mutant (-/-) heart. The mutant resembles the wild-type, except for the complete absence of ventricular trabeculae, the appearance of a slightly reduced endocardial cushion, and a noticeable swelling of both the atrium and ventricle. Many more RBCs have collected in the mutant heart chambers relative to wild-type, which is a typical feature of the poorly functioning mutant hearts. **METHODS.** E10.5 wild-type and mutant mouse embryos were fixed in 4% paraformaldehyde and subsequently embedded in paraffin. Sections were cut at 8  $\mu\text{m}$ , and were stained with haematoxylin-eosin according to standard protocols.

FIG. 4 Neural phenotype in the hindbrains of *ErbB4* mutants. *a, b*, Whole-mount (side view, anterior to the left) of TuJ1-stained wild-type (+/+) (*a*) and mutant (-/-) (*b*) embryos, respectively, at E10.5. The apparent fusion of the trigeminal (V) and facial/acoustic (VII/VIII) ganglia is marked by the brace in *b*. In addition, the caudal deflection of the IXth cranial nerve in the mutant (*IX<sub>n</sub>*) into the bundle shared by the Xth and XIth nerves (*X<sub>n</sub>* and *XI<sub>n</sub>*) is marked by the large arrow in *b*. *V<sub>op</sub>*, *V<sub>mx</sub>*, *V<sub>mn</sub>* are ophthalmic, maxillary and submandibular nerve branches from the trigeminal ganglion, respectively. *c*, A 50- $\mu$ m horizontal section through the hindbrain of a wild-type E10.5 embryo (anterior to the left), previously stained with TuJ1 as in *a*, illustrating the normal connection of the trigeminal (V) ganglion to rhombomere 2 (r2 ep), and of the facial/acoustic (VII/VIII) ganglia to rhombomere 4 (r4 ep). OV, otic vesicle. *d*, A similar section through the hindbrain of a mutant E10.5 embryo at the level of the r2 ep. The trigeminal ganglion (V) is now connected to the hindbrain at both rhombomeres 2 and 4. *e*, A more ventral section of the same embryo as shown in *d*, at the level of the facial and acoustic ganglia (VII/VIII), which are also connected at r2 and r4. (A more ventral positioning of the facial and acoustic ganglia, relative to wild-type, is a consistent feature of the *ErbB4*<sup>-/-</sup> mutants.) *f*, Dorsal view of a whole mount *in situ* hybridization reaction, performed in a mutant embryo, for the *HoxB1* gene, which remains confined to a single r4 stripe, just rostral to the otic vesicle (OV). *g*, Flat-mount confocal image of a wild-type (+/+) E10.5 mouse hindbrain dissected from a single embryo in which Dil injections were made into the trigeminal ganglion (left) and the facial ganglion (right). The approximate positions of rhombomeres 1–5 (r1–r5) are indicated. Retrogradely labelled motor neuron cell bodies lie near the floor plate (fp), and their axons project to exit points that are just ventral (in this flat-mount just medial) to the entry points (ep) of incoming sensory axons from the injected ganglion (removed during dissection). *h*, A similar flat-mount confocal image obtained from trigeminal (left side) and facial (right side) ganglion injections in an *ErbB4* mutant (-/-) embryo. Note that two sensory axon entry points (ep) are labelled from each of the single ganglion injections.



METHODS. Embryos were fixed in Dent's fixative<sup>31</sup> overnight at 4 °C, subsequently bleached in H<sub>2</sub>O<sub>2</sub>, and then incubated overnight with the TuJ1 mouse monoclonal antibody. After washing, embryos were incubated in a horseradish peroxidase (HRP)-conjugated goat anti-mouse secondary antibody overnight, and subsequent HRP reaction was performed with diaminobenzidine and hydrogen peroxide. Anterograde and retrograde axonal tracing was performed as described previously<sup>32</sup>. A solution of Dil C<sub>18</sub> (Molecular Probes D-282) was pressure injected into either the lateral trigeminal or the facial ganglion. Dil optical images were obtained by using a Bio-Rad MRC 600 confocal microscope.



and mutant embryos at E10.5 by using an antibody (TuJ1) directed against a neuron-specific tubulin isoform<sup>21</sup>. These analyses indicated a near-fusion of ganglia V and VII/VIII. In addition in some but not all mutants, we observed a caudal displacement of cranial nerve IX towards nerve X (vagal) (Fig. 4a, b). Both of these alterations are also observed in mice carrying mutations in the *Krox-20* gene<sup>22,23</sup>, which encodes a zinc-finger transcription factor which has expression restricted to r3 and r5 (ref. 24). (The caudal displacement of the IXth nerve, which may be due to the physical interference of the r6 neural-crest cell stream by a caudally displaced otic vesicle, is more robust in *Krox-20*<sup>-/-</sup> mice than in *ErbB4* mutants<sup>22,23</sup>.) Although these superficial similarities in the *Krox-20* and *ErbB4* mutant phenotypes are suggestive, *ErbB4* does not appear to regulate expression of the *Krox-20* gene, because (1) *Krox-20* mRNA is still detected in r3 and r5 in the *ErbB4* mutants (data not shown), (2) *Krox-20* is normally expressed more broadly along the dorsal-ventral axis of the neural tube than is *ErbB4*, and (3) r3 and r5 are largely intact at E10.5 in *ErbB4*<sup>-/-</sup> mice, but are almost entirely deleted by this time in *Krox-20*<sup>-/-</sup> mice<sup>22,23</sup>. That *Krox-20* may participate in the rostral-caudal regulation of the *ErbB4* gene remains a possibility.

The near-fusion of ganglia V and VII/VIII in *ErbB4*<sup>-/-</sup> mice is not, as in the *Krox-20* mutants, due to the loss of r3 and r5, but rather to aberrant innervation from and to the hindbrain. Normally, motor axons destined for the trigeminal ganglion exit, and PNS sensory axons from the trigeminal enter, the hindbrain at r2, whereas axons to and from the facial/acoustic ganglia enter and exit the hindbrain at r4 (Fig. 4c)<sup>25</sup>. In the *ErbB4* mutants, however, the trigeminal ganglion displays connections to the CNS at both r2 and r4 (Fig. 4d), and the facial and acoustic ganglia are also connected to the CNS at these same two rhombomeres (Fig. 4e). In both cases, the number of axons making up the incorrect connection is approximately the same as the number of axons in the correct connection. Because the loss of *ErbB4* in r3 and r5 leads to aberrant innervation at r2 and r4, we investigated whether in *ErbB4*<sup>-/-</sup> hindbrains r2 had acquired molecular properties of r4, or vice versa. We have found no evidence for this: markers that distinguish r2 from r4 remain appropriately restricted in their expression in *ErbB4* mutants. For example, the r4-specific homeobox gene *HoxB1* (ref. 26) is neither lost from r4 (as predicted for an r4 to r2 transformation) nor acquired by r2 (Fig. 4f). To investigate hindbrain innervation in *ErbB4* mutants in greater detail, we performed local injections of the lipophilic tracer DiI into either the trigeminal or facial ganglion of E10.5 wild-type and *ErbB4*<sup>-/-</sup> embryos. As expected, injection into the wild-type trigeminal ganglion labelled a single sensory axon projection to r2 and motor neuron cell bodies in r3, r2 and r1, whereas injection into the wild-type facial ganglion labelled a single sensory axon projection to r4 and motor neuron cell bodies in r4 and r5 (Fig. 4g). In contrast, local injection of DiI into the *ErbB4*<sup>-/-</sup> facial ganglion labelled two sensory axon entry points in r4 and r2, as well as motor neuron cell bodies and axons in r4 and r5 (their normal location) and in r1, r2 and r3 (Fig. 4h). For the facial ganglion, equal numbers of sensory axons project to the correct (r4) and incorrect (r2) targets, and equal numbers of motor neuron cell bodies are retrogradely labelled in the correct and incorrect hindbrain segments. For the aberrant connection of the trigeminal ganglion to r4 (Fig. 4h), the primary defect appears to be in sensory innervation from the PNS.

We favour the hypothesis that the mis-targeting of axons to and from r2- and r4-derived cranial ganglia in the *ErbB4*<sup>-/-</sup> hindbrain results from the loss of an *ErbB4*-dependent barrier molecule, expressed in r3 and r5, which is inhibitory to axon growth across these rhombomeres. It is possible that this barrier is *ErbB4* itself, or alternatively, that *ErbB4* activation is required for the expression of the barrier (perhaps a ligand for an Eph-related receptor). Neither *neuregulin* nor *ErbB2* gene mutants exhibit the hindbrain mis-innervation phenotype of the

*ErbB4*<sup>-/-</sup> mice. The most parsimonious interpretation of this difference is that *ErbB4* recognizes a distinct ligand in this part of the CNS. A second neuregulin-related gene has been identified and cloned<sup>27</sup>, and it is now of interest to determine whether this gene encodes a new *ErbB4* ligand. □

Received 16 August; accepted 6 October 1995.

1. Plowman, G. D. et al. *Nature* **366**, 473–475 (1993).
2. Marchionni, M. A. et al. *Nature* **362**, 312–318 (1993).
3. Carraway, K. L. R. & Burden, S. J. *Curr. Opin. Neurobiol.* **5**, 1–7 (1995).
4. Schechter, A. L. et al. *Nature* **312**, 513–516 (1984).
5. Kraus, M. H., Issing, W., Miki, T., Popescu, N. C. & Aaronson, S. A. *Proc. natn. Acad. Sci. U.S.A.* **86**, 9193–9197 (1989).
6. Plowman, G. D. et al. *Proc. natn. Acad. Sci. U.S.A.* **90**, 1746–1750 (1993).
7. Sliwkowski, M. X. et al. *J. biol. Chem.* **269**, 14661–14665 (1994).
8. Lemke, G. E. & Brookes, J. P. J. *Neurosci.* **4**, 75–83 (1984).
9. Goodearl, A. D. et al. *J. biol. Chem.* **268**, 18095–18102 (1993).
10. Wen, D. et al. *Cell* **69**, 559–572 (1992).
11. Holmes, W. E. et al. *Science* **256**, 1205–1210 (1992).
12. Falls, D. L., Rosen, K. M., Corfas, G., Lane, W. S. & Fischbach, G. D. *Cell* **72**, 801–815 (1993).
13. Tybulewicz, V. L., Crawford, C. E., Jackson, P. K., Bronson, R. T. & Mulligan, R. C. *Cell* **65**, 1153–1163 (1991).
14. Nagy, A., Rossant, J., Nagy, R., Abramow-Newerly, W. & Roder, J. C. *Proc. natn. Acad. Sci. U.S.A.* **90**, 8424–8428 (1993).
15. Corfas, G., Rosen, K. M., Aratake, H., Krauss, R. & Fischbach, G. D. *Neuron* **14**, 103–115 (1995).
16. Challice, C. E. & Viragh, S. *Tissue & Cell* **6**, 447–462 (1974).
17. Meyer, D. & Birchmeier, C. *Nature* **378**, 394–398 (1995).
18. Lee, K.-F. et al. *Nature* **378**, 386–389 (1995).
19. Lumsden, A. & Keynes, R. *Nature* **337**, 424–428 (1989).
20. Lumsden, A., Sprawson, N. & Graham, A. *Development* **113**, 1281–1291 (1991).
21. Moody, S. A., Quigg, M. S. & Frankfurter, A. J. *comp. Neurol.* **279**, 567–580 (1989).
22. Schneider-Maunoury, S. et al. *Cell* **75**, 1199–1214 (1993).
23. Swiatek, P. J. & Gridley, T. *Genes Dev.* **7**, 2071–2084 (1993).
24. Nieto, M. A., Bradley, L. C. & Wilkinson, D. G. *Development (Suppl.)* **2**, 59–62 (1991).
25. Covell, D. A. Jr & Noden, D. M. *J. comp. Neurol.* **286**, 488–503 (1989).
26. Poepperl, H. et al. *Cell* **81**, 1031–1042 (1995).
27. Chang, H. & Gilbert, W. *Soc. Neurosci. Abstr.* **20**, 1694 (1994).
28. Wilkinson, D. G. & Nieto, M. A. *Meth. Enzym.* **225**, 361–373 (1993).
29. Goulding, M. D., Chalepakis, G., Deutsch, U., Erselius, J. R. & Gruss, P. *EMBO J.* **10**, 1135–1147 (1991).
30. Lai, C. & Lemke, G. *Neuron* **6**, 691–704 (1991).
31. Dent, J. A., Polson, A. G. & Klymkowsky, M. W. *Development* **105**, 61–74 (1989).
32. Simon, H. & Lumsden, A. *Neuron* **11**, 209–220 (1993).

ACKNOWLEDGEMENTS. We thank D. Ortuño, C. Jackson and P. Burrola for technical support; J.-L. Goergen for help with blastocyst injections; M. Bronner-Fraser, D. Wilkinson and K. Chien for expert advice on the developing hindbrain and heart; C. Birchmeier, D. Meyer and K.-F. Lee for communicating results prior to publication; and M. Goulding and C. Kintner for reviews of the manuscript. This work was supported by grants from the NIH (G.L. and C.L.), a postdoctoral fellowship from the Swiss National Science Foundation (M.G.), and a predoctoral fellowship from the University of Milan (D.O.).